



Cite this: *RSC Adv.*, 2018, 8, 8856

The nano heat effect of replacing macro-particles by nano-particles in drop calorimetry: the case of core/shell metal/oxide nano-particles

A. Yakymovych,^a ^{*ab} G. Kaptay,^{cde}  H. Flandorfer,^a J. Bernardi,^f S. Schwarz^f and H. Ipser^a

Experimental results are presented here obtained by a drop calorimetric method, in which Ni and Cu particles, both in bulk and nanosized form, were dropped into a liquid Sn-3.8Ag-0.7Cu solder alloy (in wt%). The molar enthalpies of mixing of the liquid (Sn-3.8Ag-0.7Cu)-Ni(Cu) alloys were measured. An extra exothermic heat effect is observed when dropping nano-particles instead of macro-particles. This is partly due to the loss of the large surface area and the corresponding large surface enthalpy of the nano-particles before their dissolution in the liquid alloy. However, a large additional exothermic heat effect was also found in the case of Cu-nano-particles, due to the exchange chemical reaction between the Cu₂O shell of the nano-particles and liquid Sn; this is caused by the fact that the Cu-nano-particles are core-shell particles with an inner metallic Cu core and an outer Cu₂O shell. This effect is less significant for Ni nano-particles which have a thinner oxide shell.

Received 25th December 2017

Accepted 20th February 2018

DOI: 10.1039/c7ra13643a

rsc.li/rsc-advances

Introduction

Nanostructured alloys represent a relatively novel class of materials compared to the conventional bulk ones, with a number of unique and promising features that have attracted an increasing number of scientists and engineers. However, there are still many open issues related to this research topic, such as the thermodynamic stability of the nanosized structures or the changes in properties during transition of the materials from the nanosized to bulk form.

At present, it is possible to produce nanoparticles (NPs) controlling not only their size but also their shape (spheres, plates, rods, *etc.*) and internal structure (metallic, bimetallic and multicomponent metal NPs), while the main progress in studies of the characteristics of NPs is achieved only in terms of size dependent thermodynamic properties. For instance, the size-dependent changes of the melting temperature, cohesive energy, melting enthalpy and entropy were theoretically predicted and experimentally described in the literature.^{1–3} At the

same time, there are only few studies dealing with changes in various other properties of NPs caused by their shape or internal structure. For instance, there is a number of papers dealing with the investigation of optical properties of metallic^{4,5} and bimetallic NPs.^{6–8} The extinction spectra of metal nanoparticles, such as Ag nanodisks and triangular prisms, Au multirods, as well as Au shell NPs with a pinhole (several nm) structure were investigated in ref. 9. A bond-energy model for the calculation of the cohesive energy was developed in order to predict the size and shape dependency of various physical properties of metallic and bimetallic NPs with core/shell structure.¹⁰

The explosive growth in the number of studies of some classes of materials is mostly related to their prospective application. For instance, in order to promote new enhanced and customer-friendly lead-free solders, nanocomposite Sn-based alloys with minor additions of metal nanoparticles have been under intensive scientific examination.^{11–13} Unfortunately, most of these studies refer to mechanical properties^{14–18} while information related to thermophysical and thermodynamic properties as well as structural features, especially in the liquid state, is scarce.^{19–21} However, a possible industrial use requires comprehensive data on new nanosized materials with precisely controlled properties. In particular, one needs reliable information on the thermodynamic stability of the employed metal nanoparticles in the bulk solder with respect to their possible dissolution during long time use. Therefore, new studies dealing with chemical and physical properties of metal NPs in a bulk metal matrix, depending on size, shape, composition, and structure of these NPs, are demanded.

^aDepartment of Inorganic Chemistry – Functional Materials, Faculty of Chemistry, University of Vienna, Althanstr. 14, 1090 Vienna, Austria. E-mail: andriy.yakymovych@univie.ac.at

^bDepartment of Metal Physics, Ivan Franko National University, Kyrylo and Mephodyi str. 8, 79005 Lviv, Ukraine

^cDepartment of Nanotechnology, University of Miskolc, Miskolc-Egyetemváros, Hungary-3515

^dMTA-ME Materials Science Research Group, Miskolc-Egyetemváros, Hungary-3515

^eBay Zoltan Ltd on Applied Research, BAY-ENG, 2 Igloi, Miskolc, Hungary-3519

^fUniversity Service Center for Transmission Electron Microscopy, Vienna University of Technology, Wiedner Hauptstrasse 8-10, A-1040 Vienna, Austria

Table 1 Enthalpies of mixing data for the addition of bulk Cu into the liquid Sn-4.2Ag alloy; standard states: pure liquid metals

Mol. Cu dropped	Measured enthalpy	Partial molar enthalpy		Integral molar enthalpy	
$n_{\text{Cu}} (10^{-3}) \text{ mol}$	$\Delta H_{\text{Signal}}^* (\text{J mol}^{-1})$	x_{Cu}^a	$\Delta_{\text{Mix}} \bar{H}_{\text{Cu}} (\text{J mol}^{-1})$	x_{Cu}^b	$\Delta_{\text{Mix}} H (\text{J mol}^{-1})$
$T = 1073 \text{ K}$; starting amount: $n_{\text{Ag}} = 1.8224 \times 10^{-3} \text{ mol}$; $n_{\text{Sn}} = 41.8071 \times 10^{-3} \text{ mol}$					
					93
0.5684	33 518 \pm 604	0.0064	−506 \pm 958	0.0129	91 \pm 7
0.4250	33 165 \pm 513	0.0176	−858 \pm 1049	0.0223	82 \pm 11
0.4547	33 350 \pm 552	0.0272	−673 \pm 1054	0.0321	73 \pm 24
0.5055	33 081 \pm 609	0.0375	−942 \pm 1046	0.0428	62 \pm 37
0.5484	33 167 \pm 622	0.0485	−856 \pm 1049	0.0542	51 \pm 50
0.5490	32 832 \pm 656	0.0598	−1191 \pm 1038	0.0653	36 \pm 64
0.5543	32 678 \pm 659	0.0708	−1345 \pm 1033	0.0763	20 \pm 77
0.5728	32 278 \pm 673	0.0818	−1737 \pm 1021	0.0874	−1 \pm 90
0.5735	32 305 \pm 674	0.0928	−1718 \pm 1021	0.0982	−21 \pm 103
0.5861	32 147 \pm 686	0.1036	−1876 \pm 1016	0.1090	−43 \pm 115
0.6221	31 584 \pm 715	0.1146	−2439 \pm 999	0.1201	−73 \pm 128
0.6412	31 509 \pm 735	0.1258	−2514 \pm 996	0.1314	−104 \pm 141
0.6621	31 693 \pm 764	0.1370	−2330 \pm 1002	0.1427	−133 \pm 154
0.6729	31 618 \pm 774	0.1483	−2405 \pm 1000	0.1538	−163 \pm 167
0.6982	31 383 \pm 797	0.1595	−2640 \pm 992	0.1651	−196 \pm 180
0.6986	30 800 \pm 783	0.1707	−3223 \pm 974	0.1762	−236 \pm 192
0.7058	30 738 \pm 790	0.1816	−3285 \pm 972	0.1870	−276 \pm 204
0.8912	30 456 \pm 988	0.1936	−3567 \pm 963	0.2003	−330 \pm 218
0.9026	30 035 \pm 987	0.2068	−3989 \pm 950	0.2133	−389 \pm 232
$T = 873 \text{ K}$; first measurement; starting amount: $n_{\text{Ag}} = 1.7980 \times 10^{-3} \text{ mol}$; $n_{\text{Sn}} = 41.2485 \times 10^{-3} \text{ mol}$					
					168
0.2275	26 836 \pm 367	0.0026	−1445 \pm 1077	0.0053	157 \pm 8
0.2985	26 834 \pm 481	0.0087	−1448 \pm 1077	0.0121	146 \pm 19
0.3254	26 633 \pm 521	0.0157	−1648 \pm 1069	0.0194	133 \pm 31
0.3738	26 326 \pm 591	0.0235	−1955 \pm 1056	0.0277	116 \pm 44
0.3762	26 383 \pm 596	0.0318	−1898 \pm 1059	0.0359	99 \pm 57
0.4031	25 741 \pm 623	0.0402	−2541 \pm 1033	0.0445	76 \pm 71
0.4038	25 659 \pm 623	0.0487	−2622 \pm 1030	0.0530	52 \pm 84
0.4617	25 844 \pm 717	0.0577	−2437 \pm 1037	0.0625	27 \pm 98
0.4643	25 883 \pm 722	0.0672	−2398 \pm 1039	0.0719	3 \pm 113
0.4787	25 618 \pm 737	0.0766	−2663 \pm 1028	0.0814	−25 \pm 128
0.5448	25 135 \pm 823	0.0866	−3147 \pm 1009	0.0919	−61 \pm 143
0.5582	25 443 \pm 853	0.0972	−2838 \pm 1021	0.1025	−93 \pm 160
0.5697	24 608 \pm 842	0.1078	−3674 \pm 987	0.1130	−135 \pm 175
0.6367	24 833 \pm 950	0.1188	−3448 \pm 996	0.1245	−178 \pm 192
0.8346	24 284 \pm 1218	0.1318	−3997 \pm 974	0.1391	−242 \pm 213
$T = 873 \text{ K}$; second measurement; starting amount: $n_{\text{Ag}} = 1.7652 \times 10^{-3} \text{ mol}$; $n_{\text{Sn}} = 40.4961 \times 10^{-3} \text{ mol}$					
					168
0.5287	27 335 \pm 736	0.0062	−1056 \pm 994	0.0124	150 \pm 17
0.5341	26 341 \pm 717	0.0184	−2049 \pm 958	0.0245	123 \pm 33
0.5679	26 795 \pm 775	0.0308	−1595 \pm 974	0.0371	100 \pm 50
0.5970	26 517 \pm 807	0.0436	−1873 \pm 964	0.0501	74 \pm 67
0.6152	25 994 \pm 815	0.0565	−2396 \pm 945	0.0630	40 \pm 84
0.6165	26 133 \pm 821	0.0693	−2257 \pm 950	0.0757	9 \pm 101
0.6252	25 237 \pm 804	0.0819	−3153 \pm 918	0.0881	−34 \pm 117
0.6330	25 837 \pm 833	0.0943	−2553 \pm 939	0.1004	−67 \pm 132
0.6442	25 443 \pm 835	0.1065	−2947 \pm 925	0.1126	−106 \pm 148
0.6478	24 890 \pm 822	0.1185	−3500 \pm 905	0.1245	−152 \pm 163
0.6838	24 527 \pm 855	0.1306	−3863 \pm 892	0.1367	−204 \pm 178
0.7186	24 314 \pm 890	0.1429	−4076 \pm 884	0.1492	−260 \pm 193
0.7401	24 488 \pm 924	0.1554	−3902 \pm 890	0.1617	−313 \pm 208
0.7588	23 746 \pm 918	0.1679	−4644 \pm 863	0.1741	−377 \pm 222
0.7771	23 671 \pm 937	0.1803	−4719 \pm 861	0.1865	−442 \pm 237

^a Average of x_{Cu} before and after drop. ^b Per mole of the mixture.

In the present study, a drop calorimetric method is used to investigate the “thermodynamic nanoeffects”. A Sn-3.8Ag-0.7Cu alloy (SAC387; in wt%) was employed in the performed study as the main component since SAC387 is a commercially available solder. Many papers are dealing with nanocomposite Sn–Ag–Cu (SAC) solders, attempting to improve their properties by minor additions of metal NPs such as Co, Cu, Fe, Ni, *etc.*^{17,22} The nanocomposite SAC solder is reflowed during the soldering process, and reactive metal NPs are dissolved in the liquid Sn-based matrix. Therefore, the present research provides essential data to simulate the soldering process using nanocomposite solders with nano-sized metal additions in a proper way. The heat effects caused by the dissolution of Cu and Ni in bulk as well as in nanosized form were determined and the excess surface enthalpies of the employed NPs were derived. The experimental results are theoretically described taking into account not only the size but also the internal structure of the nanoparticles, *i.e.* their apparent core-shell (metal core/oxide shell) structure.

Results and discussion

Calorimetric measurements. The present study was started with calorimetric measurements, adding pieces of bulk Cu into a liquid Sn-4.2Ag alloy (in at%) (Table 1), where the molar enthalpy of mixing for the liquid Sn-4.2Ag alloy was taken from Flandorfer *et al.*²³ Since the concentration values in figures and tables are given in at%, the composition of the SAC387 master alloy is also converted to at%, resulting in a composition Sn-4.1Ag-1.3Cu. The measurements were performed at 1073 K and 873 K; they were compared with data calculated by a Redlich–Kister–Muggianu polynomial based on literature data by Luef *et al.*²⁴

Fig. 1 shows very good agreement between experimental values and calculated curves, taking into account that the experimental data of ref. 24 were obtained at temperatures different from the present ones, namely 773 K, 973 K and 1173 K. The corresponding values of the integral enthalpy of mixing for the liquid Sn-4.1Ag-1.3Cu alloy were then used as the starting values required for the evaluation of $\Delta_{\text{mix}}H$ of quaternary liquid Ag–Cu–Ni–Sn alloys. As evident from Fig. 1, the deviation

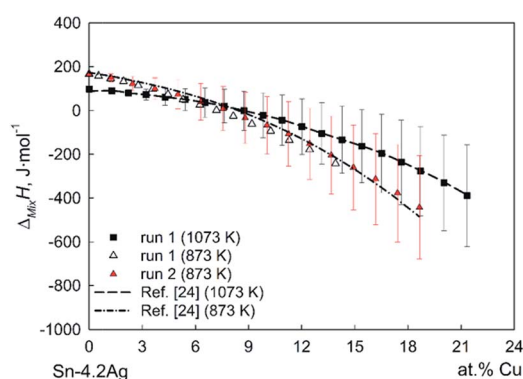


Fig. 1 Integral enthalpy of mixing of liquid (Sn-4.2Ag)_{100-x}Cu_x alloys.

from ideal behavior (enthalpy of mixing is equal to zero) is more significant at the lower temperature, in full accord with the general expectation for systems with chemical compounds.²⁵

The experimental values for the Ag–Cu–Ni–Sn system are presented in Table 2, and they are compared with literature data by Saeed *et al.*,²⁶ obtained at 1273 K, in Fig. 2. In order to describe the molar enthalpy of mixing for liquid quaternary alloys, it was suggested to modify the Redlich–Kister–Muggianu polynomial by adding an additional term corresponding to symmetric quaternary interactions.²⁶ As seen from Fig. 2, there is a reasonably good agreement between experimental and calculated data with a maximum difference of less than 1 kJ mol⁻¹.

The results in Table 3 differ from those in Tables 1 and 2 by the experimental procedure: they were obtained by dropping pieces of Cu or Ni wrapped in a Sn-4.1Ag-1.3Cu foil into the liquid alloy in the calorimeter at 1073 K and 873 K. These measurements were performed to ensure that no significant side effects would be observed when dropping NPs wrapped into such a foil into the calorimeter. As seen from Fig. 3a and b, very good agreement was obtained between experimental results with and without employing the Sn-4.1Ag-1.3Cu foil. It should also be noted that, in contrast to the ternary Ag–Cu–Sn alloys (Fig. 1), the quaternary Ag–Cu–Ni–Sn alloys did not show any significant temperature dependence of the molar mixing enthalpies (Fig. 2 and 3b). The present results of the partial enthalpy of mixing for ternary and quaternary alloys were exothermic in the investigated concentration range at both temperatures while the integral enthalpy of mixing for the ternary (Sn-4.1Ag-1.3Cu)–Cu alloys changes from positive to negative values with increasing Cu content. Furthermore, the experimental data for the ternary (Sn-4.1Ag-1.3Cu)–Cu alloys indicated a clear temperature and concentration dependence of the integral enthalpy of mixing, with a tendency to more exothermic values at lower temperatures and higher Cu contents.

The microstructure analysis of the samples after calorimetric measurements showed that the intermetallic compounds (IMCs) Ag₃Sn, Cu₆Sn₅ and Ni₃Sn₄ had been formed during the solidification of the investigated Ag–Cu–Ni–Sn samples (Fig. 4a–d, Table 4). These results are in very good agreement with the quaternary Ag–Cu–Ni–Sn phase diagram.²⁷ According to SEM analyses of the investigated samples, a substitution of Ni and Cu atoms, respectively, was observed in the IMCs Cu₆Sn₅ and Ni₃Sn₄. This effect is more pronounced for (Cu,Ni)₆Sn₅ due to a significantly increasing exothermic enthalpy of formation of this compound on admixture of Ni.²⁸ In the Sn₇₆Ag₃Cu₂₁ alloy, two Cu–Sn IMCs were found, namely Cu₃Sn and Cu₆Sn₅. According to the Cu–Sn phase diagram, Cu₃Sn should be formed in the investigated alloy during cooling and should decompose under equilibrium conditions into pure Sn and Cu₆Sn₅ at 681 K.²⁹ However, the cooling of the sample after the calorimetric measurement was certainly not slow enough to reach an equilibrium state, thus Cu₃Sn grains are left as can be seen in the microstructure.

After the experiments with bulk Cu and Ni, the corresponding experiments with nano-particles were performed (Tables 5 and 6). The excess enthalpies due to the nano-effect were



Table 2 Enthalpies of mixing data for the addition of bulk Ni into the liquid Sn-4.1Ag-1.3Cu alloy; standard states: pure liquid metals

Mol. Ni dropped	Measured enthalpy	Partial molar enthalpy		Integral molar enthalpy	
n_{Ni} (10^{-3} mol)	$\Delta H_{\text{Signal}}^*$ (J mol^{-1})	x_{Ni}^a	$\Delta_{\text{Mix}}\bar{H}_{\text{Ni}}$ (J mol^{-1})	x_{Ni}^b	$\Delta_{\text{Mix}}H$ (J mol^{-1})
$T = 1073 \text{ K}$; starting amount: $n_{\text{Ag}} = 1.6901 \times 10^{-3} \text{ mol}$; $n_{\text{Cu}} = 0.5285 \times 10^{-3} \text{ mol}$; $n_{\text{Sn}} = 38.5956 \times 10^{-3} \text{ mol}$					
					93
1.1040	-9226 ± 667	0.0132	-49894 ± 650	0.0263	-1225 ± 16
1.1889	-9214 ± 718	0.0398	-49882 ± 649	0.0532	-2567 ± 32
1.2866	-10252 ± 864	0.0669	-50920 ± 723	0.0806	-3969 ± 51
1.3084	-10061 ± 863	0.0938	-50729 ± 709	0.1069	-5307 ± 68
1.6360	-11267 ± 1208	0.1224	-51935 ± 794	0.1378	-6919 ± 91
$T = 1073 \text{ K}$; second measurement; starting amount: $n_{\text{Ag}} = 1.7825 \times 10^{-3} \text{ mol}$; $n_{\text{Cu}} = 0.5574 \times 10^{-3} \text{ mol}$; $n_{\text{Sn}} = 40.7056 \times 10^{-3} \text{ mol}$					
					93
0.2259	-9155 ± 135	0.0026	-49719 ± 643	0.0052	-169 ± 15
0.2769	-9283 ± 168	0.0084	-49848 ± 652	0.0115	-485 ± 30
0.3012	-9718 ± 191	0.0149	-50282 ± 683	0.0183	-827 ± 45
0.3641	-9669 ± 230	0.0224	-50234 ± 680	0.0264	-1234 ± 60
0.3723	-9784 ± 238	0.0305	-50349 ± 688	0.0345	-1644 ± 75
0.3743	-9825 ± 240	0.0386	-50390 ± 691	0.0426	-2050 ± 90
0.4248	-10111 ± 280	0.0471	-50676 ± 711	0.0515	-2505 ± 105
0.4646	-10129 ± 307	0.0564	-50693 ± 712	0.0612	-2993 ± 119
0.5238	-9884 ± 338	0.0665	-50449 ± 695	0.0718	-3529 ± 133
0.5556	-10511 ± 381	0.0773	-51076 ± 739	0.0828	-4092 ± 147
0.5738	-11319 ± 424	0.0883	-51884 ± 796	0.0938	-4669 ± 162
0.5936	-11034 ± 428	0.0994	-51599 ± 775	0.1050	-5249 ± 176
0.6200	-11567 ± 468	0.1107	-52132 ± 813	0.1164	-5845 ± 190
0.6274	-11251 ± 461	0.1220	-51816 ± 791	0.1276	-6430 ± 204
0.6874	-12276 ± 551	0.1336	-52841 ± 863	0.1396	-7067 ± 218
$T = 873 \text{ K}$; first measurement; starting amount: $n_{\text{Ag}} = 1.7086 \times 10^{-3} \text{ mol}$; $n_{\text{Cu}} = 0.5343 \times 10^{-3} \text{ mol}$; $n_{\text{Sn}} = 39.0184 \times 10^{-3} \text{ mol}$					
					152
0.3080	-18322 ± 397	0.0037	-52664 ± 1108	0.0074	-242 ± 10
0.3278	-18316 ± 423	0.0113	-52658 ± 1108	0.0152	-652 ± 20
0.5430	-17950 ± 686	0.0215	-52292 ± 1086	0.0278	-1312 ± 35
0.5684	-18800 ± 752	0.0342	-53142 ± 1137	0.0406	-1997 ± 53
$T = 873 \text{ K}$; second measurement; starting amount: $n_{\text{Ag}} = 3.5225 \times 10^{-3} \text{ mol}$; $n_{\text{Cu}} = 1.1015 \times 10^{-3} \text{ mol}$; $n_{\text{Sn}} = 80.4407 \times 10^{-3} \text{ mol}$					
					152
1.2447	-18830 ± 1419	0.0072	-53125 ± 1140	0.0144	-619 ± 16
1.2190	-18733 ± 1383	0.0213	-53029 ± 1135	0.0281	-1349 ± 32
0.4438	-18926 ± 509	0.0306	-53221 ± 1146	0.0331	-1610 ± 38
0.4800	-18996 ± 552	0.0357	-53291 ± 1150	0.0383	-1891 ± 44
0.4846	-18669 ± 548	0.0409	-52965 ± 1131	0.0435	-2169 ± 50
0.5128	-18822 ± 585	0.0463	-53117 ± 1140	0.0490	-2461 ± 56
0.5463	-19068 ± 631	0.0519	-53364 ± 1155	0.0548	-2770 ± 63

^a Average of x_{Ni} before and after drop. ^b Per mole of the mixture.

estimated, similarly as in ref. 19, by comparing the measured enthalpy values obtained with bulk and nanosized particles (Fig. 5 and 6).

In order to estimate values of the excess enthalpy, the concentration dependencies of the measured enthalpy for additions of Cu and Ni in bulk and nanosized form were plotted as a function of the content of the added element and extrapolated to zero. The estimated value of $\Delta H_{\text{i,nano}}^{\text{ex}}$ for Cu additions was found to be about $-17.0 \pm 1.2 \text{ kJ mol}^{-1}$ at 1073 K and $-18.5 \pm 1.3 \text{ kJ mol}^{-1}$ at 873 K (Fig. 5). The corresponding value of $\Delta H_{\text{i,nano}}^{\text{ex}}$ for Ni was found as about $-3.8 \pm 1.6 \text{ kJ mol}^{-1}$ at 1073 K and $-3.3 \pm 1.5 \text{ kJ mol}^{-1}$ at 873 K (Fig. 6).

The TEM analysis together with HAADF STEM (high angle annular dark field – scanning transmission electron

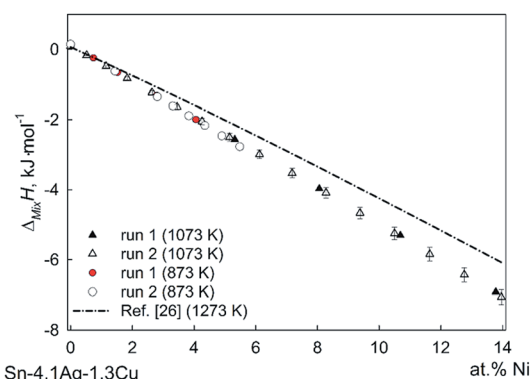
**Fig. 2** Integral enthalpy of mixing of liquid (Sn-4.1Ag-1.3Cu)_{100-x}Ni_x alloys.

Table 3 Enthalpies of mixing data for the addition of both packed bulk Cu and Ni into the liquid Sn-4.1Ag-1.3Cu alloy; standard states: pure liquid metals

Mol. packed dropped metal	Measured enthalpy	Partial molar enthalpy	Integral molar enthalpy	
n_{Cu} (10^{-3} mol)	$\Delta H_{\text{Signal}}^*$ (J mol^{-1})	x_{Cu}^a	$\Delta_{\text{Mix}}\bar{H}_{\text{Cu}}$ (J mol^{-1})	x_{Cu}^b
$T = 1073 \text{ K}$; starting amount: $n_{\text{Ag}} = 2.0639 \times 10^{-3} \text{ mol}$; $n_{\text{Cu}} = 0.6454 \times 10^{-3} \text{ mol}$; $n_{\text{Sn}} = 47.1327 \times 10^{-3} \text{ mol}$				
0.6101	33 431 \pm 654	0.0060	−427 \pm 1072	0.0121
0.6273	33 021 \pm 692	0.0181	−837 \pm 1103	0.0241
0.6580	32 527 \pm 722	0.0302	−1331 \pm 1098	0.0363
0.6816	32 532 \pm 761	0.0425	−1326 \pm 1117	0.0486
0.7116	32 707 \pm 790	0.0548	−1151 \pm 1110	0.0610
0.7181	32 267 \pm 821	0.0670	−1592 \pm 1144	0.0731
0.7284	32 090 \pm 789	0.0790	−1768 \pm 1083	0.0849
0.7326	32 363 \pm 787	0.0907	−1495 \pm 1075	0.0965
0.7487	31 614 \pm 862	0.1022	−2244 \pm 1152	0.1079
0.7657	31 775 \pm 857	0.1135	−2083 \pm 1119	0.1191
0.7762	31 465 \pm 813	0.1247	−2393 \pm 1048	0.1302
0.7933	31 575 \pm 877	0.1357	−2284 \pm 1105	0.1411
0.8448	31 104 \pm 859	0.1468	−2754 \pm 1017	0.1525
0.8656	31 181 \pm 893	0.1582	−2677 \pm 1031	0.1638
0.8783	30 703 \pm 853	0.1694	−3155 \pm 971	0.1750
0.9206	30 828 \pm 906	0.1807	−3030 \pm 984	0.1864
0.9556	30 679 \pm 965	0.1920	−3179 \pm 1010	0.1976
0.9794	30 405 \pm 1046	0.2031	−3453 \pm 1068	0.2086
1.1165	29 964 \pm 972	0.2149	−3894 \pm 871	0.2213
1.1578	29 959 \pm 960	0.2278	−3900 \pm 830	0.2343
$T = 1073 \text{ K}$; starting amount: $n_{\text{Ag}} = 3.6576 \times 10^{-3} \text{ mol}$; $n_{\text{Cu}} = 1.1436 \times 10^{-3} \text{ mol}$; $n_{\text{Sn}} = 83.5197 \times 10^{-3} \text{ mol}$				
0.2961	−9558 \pm 68	0.0017	−50193 \pm 228	0.0033
0.6407	−9529 \pm 281	0.0069	−50164 \pm 438	0.0105
0.7048	−9220 \pm 337	0.0144	−49855 \pm 478	0.0182
0.8726	−10072 \pm 464	0.0229	−50707 \pm 532	0.0276
0.9016	−10140 \pm 420	0.0324	−50775 \pm 465	0.0371
0.9177	−9371 \pm 404	0.0419	−50006 \pm 441	0.0466
0.9838	−9552 \pm 509	0.0516	−50187 \pm 517	0.0566
0.9888	−10474 \pm 466	0.0615	−51109 \pm 472	0.0663
1.0563	−10137 \pm 492	0.0714	−50772 \pm 466	0.0765
1.1982	−11081 \pm 565	0.0821	−51716 \pm 472	0.0878
1.3312	−10262 \pm 674	0.0939	−50897 \pm 506	0.1000
$T = 873 \text{ K}$; starting amount: $n_{\text{Ag}} = 3.5799 \times 10^{-3} \text{ mol}$; $n_{\text{Cu}} = 1.1194 \times 10^{-3} \text{ mol}$; $n_{\text{Sn}} = 81.7527 \times 10^{-3} \text{ mol}$				
0.5236	−18437 \pm 498	0.0030	−52800 \pm 950	0.0060
0.7791	−18687 \pm 752	0.0104	−53050 \pm 966	0.0148
0.8281	−18514 \pm 860	0.0194	−52877 \pm 1038	0.0240
0.8751	−19025 \pm 878	0.0287	−53388 \pm 1003	0.0335
0.9304	−18348 \pm 906	0.0384	−52711 \pm 974	0.0434

microscopy) imaging should bring essential information about the characteristics of the employed Cu and Ni NPs in order to explain the significant difference in the values of the excess surface enthalpy. Fig. 7 and 8 show examples of the TEM micrographs of Cu and Ni NPs which show that the NPs (including oxide shell) are of similar size, considering the original size distribution.

Furthermore, EDX elemental mapping of Cu NPs showed an oxide shell (Cu_2O) covering a metal core (Fig. 7(a–c)). These data are in a good agreement with XRD analysis indicating the presence of both Cu and Cu_2O (cubic, see ref. 30) in the investigated Cu nanopowder (Fig. 9a). In the case of Ni NPs, only traces of NiO (trigonal/rhombohedral, see ref. 31) with very low intensity were found in the XRD pattern (Fig. 9b); only minor



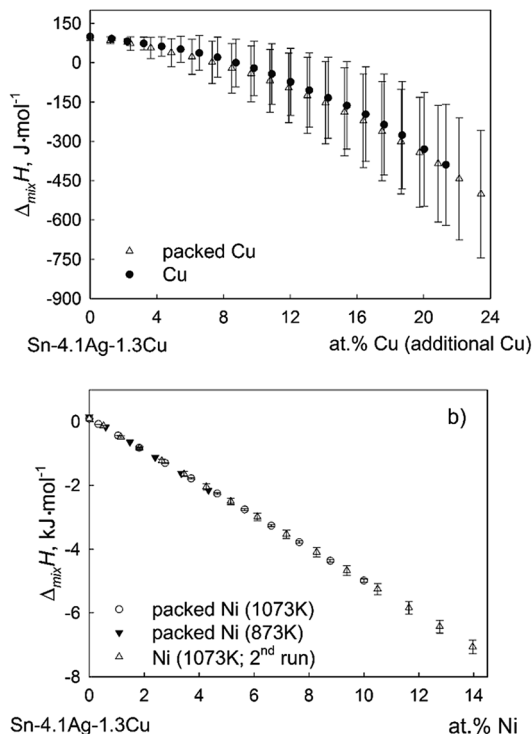


Fig. 3 Integral enthalpy of mixing of liquid (Sn-4.1Ag-1.3Cu)_{100-x}Cu_x alloys at 1073 K (a) and (Sn-4.1Ag-1.3Cu)_{100-x}Ni_x alloys at 1073 K and 873 K (b).

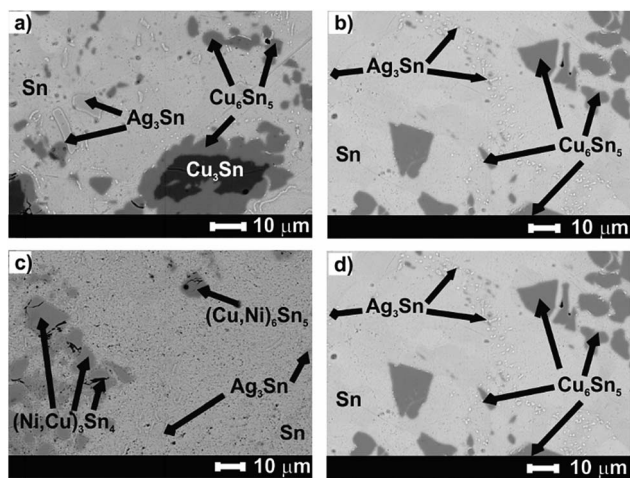


Fig. 4 BSE micrographs of (Sn-4.1Ag-1.3Cu)_{100-x}Cu_x (a) – Sn₇₆Ag₃–Cu₂₁; (b) – Sn₈₃Ag₄Cu₁₃) and (Sn-4.1Ag-1.3Cu)_{100-x}Ni_x (c) – Sn₈₁Ag₄–Cu₁Ni₁₄; (d) – Sn₉₁Ag₄Cu₁Ni₄) samples after calorimetry.

amounts of oxygen were found on the surface of the Ni NPs (Fig. 8b and c). The first broad peak in the X-ray patterns is caused by the specimen holder with the polycarbonate cap.

Pore size distributions of Cu and Ni NPs were measured by nitrogen sorption according to the theory of Barrett, Joyner and Halenda (BJH) (Fig. 10a and b). The determined BET surface area of the employed NPs is equal to $(10.6 \pm 0.4) \times 10^3 \text{ m}^2 \text{ kg}^{-1}$ for Cu NPs and $(10.2 \pm 0.4) \times 10^3 \text{ m}^2 \text{ kg}^{-1}$ for Ni NPs.

Theoretical considerations

The goal of this chapter is to model the observed $\Delta H_{i,nano}^{ex}$ values by applying the principles of nano-thermodynamics.^{32–34} In a previous paper¹⁹ the nano-effect was described as

$$\Delta H_{i,nano}^{ex} = -A_{BET} M \sigma_{sg,H,T_D}, \quad (1)$$

where A_{BET} ($\text{m}^2 \text{ g}^{-1}$) is the BET surface area of the nano-particles (which is assumed to be negligible for bulk material), M (g mol^{-1}) is the molar mass of the nano-particles, σ_{sg,H,T_D} (J m^{-2}) is the enthalpy part of the surface energy of the solid nano-particles at the drop temperature. (Note that in the present paper the sign of $\Delta H_{i,nano}^{ex}$ is kept positive contrary to the previous paper,¹⁹ thus a negative sign appears in eqn (1); this is done for two reasons: to avoid predicting anything before the experiments are run, and to make more obvious that the nano-effect is exothermic). The physical meaning of eqn (1) is the loss (see the negative sign) of the enthalpy part of the surface energy of the nano-particles upon dissolution per mole of metal added. The calculated and experimental results for the systems studied in this paper are compared in Table 7.

As follows from Table 7, the experimental values in this case are considerably more negative than the calculated ones, and this difference is especially striking for Cu nanoparticles. This is most probably due to the fact that eqn (1) is strictly valid only for pure metallic nano-particles without any oxide shell. However, as observed by the TEM and XRD investigations of the nano-particles (see Fig. 6–8), the Cu-nano-particles are severely contaminated by oxygen. Actually, instead of Cu-nano-particles we have core/shell nano-particles with a Cu inner core (α) and a Cu₂O shell (β), which form together particle γ . A similar oxidation problem exists also for Ni nano-particles, however, to a much smaller extent. Therefore, the previous model in eqn (1) has to be modified to take into account the role of the oxide shells on the metallic nano-particles, too.

When the experiments were performed, it was assumed that n_{Me}^0 (mole) of pure metal was added into the calorimeter. Instead, the molar part y of these nano-particles was actually oxidized so that in fact the following amounts of matter were added:

$$n_{\alpha} = (1 - y)n_{Me}^0, \quad (2)$$

$$n_{\beta} = yn_{Me}^0, \quad (3)$$

where α denotes the added metal, and β denotes its oxide shell MeO_x (where the stoichiometry is always written such that the oxide molecule contains one metallic atom, i.e., x can be any positive number). Thus, in addition to eqn (1), there are two additional terms for the enthalpy nano-effect: one is responsible for different heat capacities of α (metal) and β (oxide), while the other one is responsible for the chemical interaction between β and metal atoms in the liquid alloy (in our case these are mostly atoms of Sn), into which the nano-particles are added:

$$\Delta H_{\alpha/\beta,nano}^{ex} = -A_{BET} M_{\gamma} \sigma_{\gamma,H,T_D} + y(\Delta H_{C_p} + \Delta_r H^0), \quad (4)$$

Table 4 SEM-EDX results of (Sn-4.1Ag-1.3Cu)_{100-x}Cu_x and (Sn-4.1Ag-1.3Cu)_{100-x}Ni_x samples after calorimetry

Sample	Temperature of calor. meas. (K)	Dropped component	Phase 1		Phase 2			Phase 3			Phase 4			
			Sn at%		Ag at%	Sn at%		Cu at%	Ni at%	Sn at%		Ni at%	Cu at%	Sn at%
Sn ₇₆ Ag ₃ Cu ₂₁ 1st meas.	1073	bulk Cu	βSn	100	Ag ₃ Sn	75	25	Cu ₆ Sn ₅	53	—	47	—	—	—
Sn ₈₃ Ag ₄ Cu ₁₃ 2nd meas.	873	nano Cu	βSn	100	Ag ₃ Sn	73	27	Cu ₃ Sn	74	—	26	—	—	—
Sn ₈₃ Ag ₄ Cu ₁₃ 2nd meas.								Cu ₆ Sn ₅	53	—	47	—	—	—
Sn ₈₁ Ag ₄ Cu ₁ Ni ₁₄ 1st meas.	1073	bulk Ni	βSn	100	Ag ₃ Sn	76	24	(Cu,Ni) ₆ Sn ₅	34	18	48	(Ni,Cu) ₃ Sn ₄	39	3
Sn ₉₁ Ag ₄ Cu ₁ Ni ₄ 1st meas.	873	nano Ni	βSn	100	Ag ₃ Sn	73	27	(Cu,Ni) ₆ Sn ₅	34	19	50	(Ni,Cu) ₃ Sn ₄	40	2
Sn ₉₁ Ag ₄ Cu ₁ Ni ₄ 1st meas.														58

where M_γ is the average molar mass of the partly oxidized particle as defined by eqn (5), σ_{γ,H,T_D} is the effective enthalpy part of the surface energy of the partly oxidized particle as defined by eqn (6), and ΔH_{C_p} (J mol⁻¹) is the enthalpy difference due to the different heat capacities of the oxide and the metal as defined by eqn (7); $\Delta_r H^0$ (J mol⁻¹) is the standard molar enthalpy change of the chemical reaction: $MeO_x + ySn = Sn_yO_x + Me$ (or, which is the same: $\beta + ySn = Sn_yO_x + \alpha$, where the stoichiometry is always written such that the oxide molecule contains one metallic atom, *i.e.*, x can be any positive number):

$$M_\gamma = (1 - y)M_\alpha + yM_\beta, \quad (5)$$

$$\sigma_{\gamma,H,T_D} \cong \sigma_{\alpha/\beta,H,T_D} + \sigma_{\beta,H,T_D} + \left(\sigma_{\alpha,H,T_D} - \sigma_{\alpha/\beta,H,T_D} - \sigma_{\beta,H,T_D} \right) \exp\left(-\frac{d}{\delta}\right), \quad (6)$$

$$\Delta H_{C_p} = \int_{T_D}^{T_M} (C_{p,\beta} - C_{p,\alpha})dT, \quad (7)$$

where M_α (g mol⁻¹) is the molar mass of the metal core, M_β (g mol⁻¹) is the molar mass of the oxide shell, $\sigma_{\alpha/\beta,H,T_D}$ (J m⁻²) is the enthalpy part of the α/β interfacial energy, σ_{β,H,T_D} (J m⁻²) is the enthalpy part of the surface energy of the oxide shell, σ_{α,H,T_D} (J m⁻²) is the enthalpy part of the surface energy of the metallic core, d (nm) is the thickness of the oxide shell, $\delta \cong 1$ nm is the coefficient in the separation dependence of interfacial energies,³⁶ $C_{p,\beta}$ (J (mol K)⁻¹) is the molar heat capacity of the oxide shell of the nano-particle, $C_{p,\alpha}$ (J (mol K)⁻¹) is the molar heat capacity of the metallic inner core of the nano-particle. When the oxide shell is thin, it is modelled as a shell of constant thickness following the original shape of the nano-particle. If this thickness is much smaller than the radius of the nano-particle, the BET surface area of the outer oxide/gas surface and the BET interfacial area of the inner metal/oxide interface are considered equal.

In order to check whether the proposed reactions are exergonic and favorable or not, the free energy change for the reactions was estimated from the Gibbs energy of formation values of the oxides of copper ($\Delta_r G_{Cu_2O}$), nickel ($\Delta_r G_{NiO}$) and tin ($\Delta_r G_{SnO_2}$). In the present case, there are two chemical exchange reactions, *i.e.* $(Cu_2O + 1/2Sn = 1/2SnO_2 + 2Cu)$ and $(NiO + 1/2Sn = 1/2SnO_2 + Ni)$. It is assumed that the Gibbs energy change for the first reaction can be obtained as $\Delta_r G_{(NiO/SnO_2)} = 1/$

$2\Delta_r G_{SnO_2} - \Delta_r G_{NiO}$ and that for the second reaction as $\Delta_r G_{(Cu_2O/SnO_2)} = 1/2\Delta_r G_{SnO_2} - \Delta_r G_{Cu_2O}$. The Gibbs energies of formation for the oxides at 1073 K and 873 K were taken from ref. 37 and 38. Based on the obtained results, the calculated Gibbs energy change for the reactions is exothermic at both temperatures and equals -93.3 kJ mol⁻¹ and -86.9 kJ mol⁻¹ for $\Delta_r G_{(Cu_2O/SnO_2)}$, and -38.2 kJ mol⁻¹ and -34.5 kJ mol⁻¹ for $\Delta_r G_{(NiO/SnO_2)}$ at 873 K and 1073 K, respectively.

The amount of matter of the oxide shell can be expressed from its geometry as:

$$n_\beta \cong A_{BET} d \rho_\beta n_{Me}^0, \quad (8)$$

where ρ_β (g m⁻³) is the density of the oxide shell. The quantities expressed by eqn (3) and (8) are equal. Consequently, the thickness of the oxide shell (d) can be expressed as function of the mole fraction of the oxidized part of the nano-particle (y), as:

$$d \cong \frac{y}{A_{BET} \rho_\beta}. \quad (9)$$

Let us also mention that for $y = 0$, eqn (4) becomes identical to eqn (1), being a reasonable boundary condition. Substituting eqn (5)–(7) and (9) into eqn (4), the excess nano heat effect can be calculated as function of y for partly oxidized metallic nano-particles.

The corresponding constants are given in Table 7. In this paper, the selection Sn was made (for the values in the last column of Table 8), as Sn has the highest affinity towards oxygen and the highest mole fraction in the liquid alloy among its components (Sn, Cu, Ag). The results calculated based on Table 8 are compared with experimental data in Fig. 11 and 12.

As follows from Fig. 11 and 12, the experimental results can be reproduced with $y = 0.24 \pm 0.02$ for Cu-nanoparticles and with $y = 0.039 \pm 0.004$ for Ni-nanoparticles. These values are in qualitative agreement with Fig. 7–9. Thus, our new extended model is able to describe the nano heat effect for the dissolution of partly oxidized nano-particles.

Experimental

The heat effects of small additions of Cu and Ni to the liquid SAC387 alloy were investigated by a drop calorimetric



Table 5 Enthalpies of mixing data for the addition of nano Cu into the liquid Sn-4.1Ag-1.3Cu alloy; standard states: pure liquid metals

Mol nano-sized Cu dropped	Measured enthalpy	Partial molar enthalpy		Integral molar enthalpy	
n_{Cu} (10^{-3} mol)	$\Delta H_{\text{Signal}}^*$ (J mol $^{-1}$)	x_{Cu}^a	$\Delta_{\text{Mix}}\bar{H}_{\text{Cu}}$ (J mol $^{-1}$)	x_{Cu}^b	$\Delta_{\text{Mix}}H$ (J mol $^{-1}$)
$T = 1073$ K; first measurement; starting amount: $n_{\text{Ag}} = 1.9452 \times 10^{-3}$ mol; $n_{\text{Cu}} = 0.6083 \times 10^{-3}$ mol; $n_{\text{Sn}} = 44.4216 \times 10^{-3}$ mol					
					93
0.2233	34 199 \pm 637	0.0024	14 \pm 1104	0.0047	91 \pm 13
0.2161	33 758 \pm 629	0.0069	−427 \pm 1127	0.0091	9 \pm 26
0.2504	34 010 \pm 633	0.0116	−175 \pm 979	0.0141	−68 \pm 39
0.2546	33 692 \pm 627	0.0166	−492 \pm 954	0.0191	−157 \pm 51
0.2747	33 839 \pm 630	0.0217	−346 \pm 888	0.0243	−243 \pm 63
0.2747	33 463 \pm 623	0.0268	−722 \pm 878	0.0294	−337 \pm 74
0.3087	33 676 \pm 627	0.0321	−509 \pm 787	0.0349	−426 \pm 85
0.3298	33 606 \pm 622	0.0378	−579 \pm 735	0.0407	−524 \pm 96
0.3360	33 156 \pm 617	0.0436	−1029 \pm 712	0.0464	−629 \pm 106
0.3482	33 233 \pm 619	0.0493	−952 \pm 688	0.0522	−733 \pm 116
0.3544	33 470 \pm 623	0.0551	−715 \pm 681	0.0580	−836 \pm 126
0.3562	32 910 \pm 613	0.0609	−1275 \pm 666	0.0637	−943 \pm 136
0.3624	33 115 \pm 617	0.0665	−1069 \pm 659	0.0692	−1047 \pm 145
0.3691	32 364 \pm 603	0.0719	−1821 \pm 632	0.0746	−1151 \pm 153
0.3913	33 257 \pm 619	0.0775	−928 \pm 613	0.0803	−1250 \pm 161
0.3954	32 276 \pm 601	0.0831	−1909 \pm 589	0.0860	−1358 \pm 169
0.4237	33 125 \pm 617	0.0889	−1059 \pm 564	0.0918	−1462 \pm 177
0.4345	32 461 \pm 604	0.0946	−1724 \pm 539	0.0974	−1571 \pm 184
0.6205	32 701 \pm 609	0.1014	−1483 \pm 380	0.1054	−1677 \pm 190
$T = 1073$ K; second measurement; starting amount: $n_{\text{Ag}} = 1.9755 \times 10^{-3}$ mol; $n_{\text{Cu}} = 0.6177 \times 10^{-3}$ mol; $n_{\text{Sn}} = 45.1128 \times 10^{-3}$ mol					
					93
0.2332	33 688 \pm 794	0.0024	−170 \pm 882	0.0048	90 \pm 16
0.1613	33 499 \pm 789	0.0064	−359 \pm 1296	0.0081	6 \pm 32
0.1933	33 488 \pm 789	0.0100	−370 \pm 1058	0.0119	−51 \pm 48
0.2653	33 506 \pm 789	0.0144	−353 \pm 772	0.0170	−119 \pm 63
0.2273	33 140 \pm 781	0.0191	−718 \pm 891	0.0212	−209 \pm 77
0.2760	33 028 \pm 778	0.0237	−830 \pm 731	0.0262	−286 \pm 91
0.3389	33 049 \pm 779	0.0292	−810 \pm 596	0.0322	−377 \pm 105
0.1684	33 079 \pm 779	0.0336	−779 \pm 1200	0.0350	−484 \pm 118
0.2893	32 908 \pm 775	0.0375	−951 \pm 695	0.0399	−536 \pm 131
0.3051	32 717 \pm 771	0.0424	−1142 \pm 655	0.0449	−626 \pm 143
0.2855	32 876 \pm 774	0.0472	−982 \pm 703	0.0495	−717 \pm 155
0.3051	32 934 \pm 776	0.0519	−925 \pm 659	0.0543	−799 \pm 167
0.3317	32 732 \pm 771	0.0569	−1126 \pm 603	0.0594	−888 \pm 178
0.3277	32 491 \pm 765	0.0618	−1367 \pm 606	0.0643	−981 \pm 189
0.3157	32 893 \pm 775	0.0665	−965 \pm 636	0.0688	−1070 \pm 200
0.3024	32 243 \pm 760	0.0709	−1615 \pm 651	0.0730	−1154 \pm 210
0.3711	32 069 \pm 755	0.0756	−1789 \pm 528	0.0782	−1237 \pm 220
$T = 873$ K; first measurement; starting amount: $n_{\text{Ag}} = 1.8702 \times 10^{-3}$ mol; $n_{\text{Cu}} = 0.5848 \times 10^{-3}$ mol; $n_{\text{Sn}} = 42.7094 \times 10^{-3}$ mol					
					152
0.1134	26 783 \pm 570	0.0012	−1597 \pm 1335	0.0025	144 \pm 13
0.1199	26 873 \pm 572	0.0038	−1508 \pm 1266	0.0051	93 \pm 25
0.1321	26 885 \pm 572	0.0065	−1495 \pm 1150	0.0079	39 \pm 37
0.1296	26 849 \pm 570	0.0092	−1532 \pm 1171	0.0106	−20 \pm 49
0.1338	27 048 \pm 576	0.0120	−1332 \pm 1143	0.0134	−75 \pm 61
0.1379	26 691 \pm 568	0.0147	−1689 \pm 1094	0.0161	−133 \pm 72
0.1462	26 922 \pm 573	0.0176	−1458 \pm 1041	0.0190	−190 \pm 83
0.1501	26 819 \pm 571	0.0205	−1562 \pm 1009	0.0220	−251 \pm 95
0.1519	26 460 \pm 563	0.0235	−1921 \pm 984	0.0249	−313 \pm 105
0.1677	26 439 \pm 563	0.0265	−1942 \pm 891	0.0281	−375 \pm 116
0.1779	26 667 \pm 568	0.0298	−1714 \pm 847	0.0314	−442 \pm 126
0.1892	26 616 \pm 566	0.0332	−1765 \pm 795	0.0349	−511 \pm 136
0.1914	26 425 \pm 562	0.0366	−1956 \pm 780	0.0383	−584 \pm 146
0.1980	26 148 \pm 557	0.0401	−2233 \pm 746	0.0418	−658 \pm 156
0.2129	25 925 \pm 552	0.0437	−2455 \pm 688	0.0455	−734 \pm 164
0.2246	26 184 \pm 557	0.0474	−2197 \pm 659	0.0494	−813 \pm 174
0.2343	26 097 \pm 555	0.0513	−2284 \pm 630	0.0533	−895 \pm 182



Table 5 (Contd.)

Mol nano-sized Cu dropped	Measured enthalpy	Partial molar enthalpy		Integral molar enthalpy	
n_{Cu} (10^{-3} mol)	$\Delta H_{\text{Signal}}^*$ (J mol^{-1})	x_{Cu}^a	$\Delta_{\text{Mix}} \bar{H}_{\text{Cu}}$ (J mol^{-1})	x_{Cu}^b	$\Delta_{\text{Mix}} H$ (J mol^{-1})
0.3362	26 195 \pm 558	0.0561	−2186 \pm 440	0.0589	−981 \pm 190
0.3904	25 837 \pm 550	0.0621	−2544 \pm 374	0.0653	−1104 \pm 198
0.0850	25 601 \pm 545	0.0658	−2780 \pm 1702	0.0664	−1234 \pm 206
$T = 873$ K; second measurement; starting amount: $n_{\text{Ag}} = 1.9152 \times 10^{-3}$ mol; $n_{\text{Cu}} = 0.5989 \times 10^{-3}$ mol; $n_{\text{Sn}} = 43.7365 \times 10^{-3}$ mol					
0.3188	27 210 \pm 571	0.0034	−1143 \pm 953	0.0068	152
0.3780	26 649 \pm 559	0.0107	−1704 \pm 787	0.0146	140 \pm 12
0.4031	26 564 \pm 557	0.0185	−1789 \pm 736	0.0225	−2 \pm 24
0.4044	26 627 \pm 559	0.0264	−1725 \pm 735	0.0225	−164 \pm 35
0.4038	26 629 \pm 559	0.0340	−1723 \pm 736	0.0303	−329 \pm 45
0.4165	26 253 \pm 551	0.0414	−2100 \pm 706	0.0377	−489 \pm 55
0.4239	26 231 \pm 550	0.0488	−2122 \pm 691	0.0452	−646 \pm 65
0.4250	25 600 \pm 537	0.0560	−2753 \pm 672	0.0525	−803 \pm 75
0.4375	25 995 \pm 545	0.0630	−2358 \pm 663	0.0595	−961 \pm 83
0.4487	25 936 \pm 544	0.0700	−2416 \pm 645	0.0665	−1113 \pm 92
0.4675	25 889 \pm 543	0.0770	−2464 \pm 618	0.0735	−1263 \pm 100
0.4745	25 845 \pm 542	0.0840	−2508 \pm 608	0.0806	−1413 \pm 108
0.4820	25 517 \pm 535	0.0909	−2835 \pm 591	0.0875	−1565 \pm 116
0.4834	25 315 \pm 531	0.0976	−3038 \pm 584	0.0943	−1717 \pm 123
0.4838	25 371 \pm 532	0.1042	−2981 \pm 585	0.1010	−1867 \pm 130
0.4957	25 077 \pm 526	0.1104	−3276 \pm 565	0.1073	−2015 \pm 137
0.5133	25 438 \pm 534	0.1167	−2915 \pm 553	0.1135	−2157 \pm 143
0.5271	24 826 \pm 521	0.1231	−3527 \pm 526	0.1199	−2295 \pm 149
0.5745	25 129 \pm 527	0.1297	−3223 \pm 488	0.1263	−2440 \pm 155
				0.1330	−2583 \pm 160

^a Average of x_{Cu} before and after drop. ^b Per mole of the mixture.

method. The measurements were carried out using a Calvet-type twin microcalorimeter system under high purity Ar (99.9999%) flow (approximately 20–30 ml min^{−1}). The apparatus consists of two thermopiles containing more than 200 thermocouples, a commercial wire wound resistance furnace (HTC-1000, SETARAM, Lyon, France) and a self-made automatic drop device for up to 30 drops. The SAC387 alloy was placed in a BN crucible. The time interval between individual drops was 40 min, and the acquisition interval of the heat flow was 0.5 s. The calorimeter was calibrated by five drops of standard $\alpha\text{-Al}_2\text{O}_3$ provided by NIST (National Institute of Standards and Technology, Gaithersburg, MD) at the end of the drop series of each separate measurement. The microcalorimeter and the mechanical sampler were controlled through a self-provided software using the graphical programming environment LabVIEW. The obtained signals from the thermocouples were recorded and evaluated using the commercial HiQ[®] software. The microcalorimeter was described in detail elsewhere.⁴²

In general, the measured enthalpy (integrated heat flow at constant pressure) for bulk materials is equal to:

$$(\Delta H_{\text{Signal}})_{\text{bulk}} = n_i (\Delta H_{\text{Signal}}^*)_{\text{bulk}} = n_i (H_{\text{m},i,T_M} - H_{\text{m},i,T_D}) + \Delta H_{\text{Reaction}}, \quad (10)$$

where n_i is the number of moles of the added element i , $\Delta H_{\text{Signal}}^*$ is the measured enthalpy in J mol^{−1}, H_{m} denotes molar

enthalpies, T_D is the drop temperature, and T_M is the calorimeter temperature for the respective measurement in Kelvin. The molar enthalpy difference $(H_{\text{m},i,T_M} - H_{\text{m},i,T_D})$ was calculated using the SGTE data for pure elements.⁴³

However, in the case of nanosized additions one must also take into account the additional heat effect caused by the excess (surface) enthalpy of the metal nanoparticles. Thus, eqn (10) for the addition in the nanosized form can be rewritten as¹⁹:

$$(\Delta H_{\text{Signal}})_{\text{nano}} = n_i \left[(\Delta H_{\text{Signal}}^*)_{\text{bulk}} + \Delta H_{\text{i,nano}}^{\text{ex}} \right] = n_i (H_{\text{m},i,T_M} - H_{\text{m},i,T_D}) + \Delta H_{\text{Reaction}} + n_i \Delta H_{\text{i,nano}}^{\text{ex}}, \quad (11)$$

where $\Delta H_{\text{i,nano}}^{\text{ex}}$ is the excess enthalpy connected with the replacement of bulk material by nano-particles in J mol^{−1}. Therefore, in order to find the heat effect caused by the additions of material in nanosized form we must know the heat effect caused by the addition of the same material in bulk form.

Furthermore, due to the rather small masses of added component i , partial enthalpies can be calculated by:

$$\Delta_{\text{Mix}} \bar{H}_i \approx \frac{\Delta H_{\text{Reaction}}}{n_i}. \quad (12)$$

The integral molar enthalpy of mixing, $\Delta_{\text{Mix}} H$, was calculated by summing the respective reaction enthalpies and dividing by



Table 6 Enthalpies of mixing data for the addition of nano Ni into the liquid Sn-4.1Ag-1.3Cu alloy; standard states: pure liquid metals

mol nano-sized Ni dropped	Measured enthalpy	Partial molar enthalpy		Integral molar enthalpy	
n_{Ni} (10^{-3} mol)	$\Delta H_{\text{Signal}}^*$ (J mol $^{-1}$)	x_{Ni}^a	$\Delta_{\text{Mix}}\bar{H}_{\text{Ni}}$ (J mol $^{-1}$)	x_{Ni}^b	$\Delta_{\text{Mix}}H$ (J mol $^{-1}$)
$T = 1073$ K; first measurement; starting amount: $n_{\text{Ag}} = 3.6656 \times 10^{-3}$ mol; $n_{\text{Cu}} = 1.1462 \times 10^{-3}$ mol; $n_{\text{Sn}} = 83.7083 \times 10^{-3}$ mol					
					93
0.7417	-13861 ± 554	0.0041	-49400 ± 543	0.0083	-318 ± 5
0.7656	-13684 ± 547	0.0124	-49222 ± 516	0.0166	-759 ± 9
0.7858	-13867 ± 555	0.0207	-49406 ± 512	0.0248	-1200 ± 14
1.1022	-13626 ± 545	0.0305	-49164 ± 357	0.0361	-1787 ± 18
0.9587	-13915 ± 556	0.0409	-49453 ± 422	0.0456	-2300 ± 22
0.9615	-13856 ± 554	0.0502	-49394 ± 418	0.0548	-2793 ± 26
1.1326	-14329 ± 573	0.0601	-49867 ± 372	0.0653	-3350 ± 30
1.1366	-14293 ± 572	0.0704	-49832 ± 369	0.0754	-3897 ± 34
1.1458	-13471 ± 539	0.0804	-49010 ± 338	0.0853	-4421 ± 37
1.1778	-14456 ± 578	0.0902	-49994 ± 362	0.0951	-4947 ± 41
1.2029	-14130 ± 565	0.0999	-49669 ± 343	0.1047	-5467 ± 44
1.2095	-14599 ± 584	0.1095	-50137 ± 357	0.1142	-5978 ± 48
1.2590	-14164 ± 566	0.1189	-49702 ± 329	0.1236	-6483 ± 51
1.2684	-15096 ± 604	0.1281	-50635 ± 356	0.1326	-6979 ± 54
1.3939	-14345 ± 574	0.1375	-49884 ± 303	0.1424	-7503 ± 57
1.4623	-15264 ± 610	0.1474	-50803 ± 314	0.1523	-8048 ± 60
1.4931	-15142 ± 606	0.1572	-50681 ± 304	0.1621	-8582 ± 63
1.5044	-14769 ± 591	0.1668	-50308 ± 292	0.1715	-9098 ± 64
$T = 1073$ K; second measurement; starting amount: $n_{\text{Ag}} = 1.7663 \times 10^{-3}$ mol; $n_{\text{Cu}} = 0.5523 \times 10^{-3}$ mol; $n_{\text{Sn}} = 40.3348 \times 10^{-3}$ mol					
					93
0.4599	-13541 ± 587	0.0053	-49053 ± 918	0.0106	-428 ± 10
0.4871	-13539 ± 587	0.0160	-49051 ± 866	0.0214	-1000 ± 20
0.5091	-13755 ± 596	0.0268	-49267 ± 847	0.0323	-1578 ± 30
0.5175	-13421 ± 581	0.0376	-48933 ± 805	0.0429	-2141 ± 39
0.5516	-13324 ± 577	0.0484	-48836 ± 748	0.0539	-2718 ± 47
0.6021	-13307 ± 577	0.0596	-48820 ± 684	0.0654	-3322 ± 55
0.6275	-14081 ± 610	0.0711	-49594 ± 710	0.0769	-3940 ± 64
0.6496	-13815 ± 599	0.0826	-49327 ± 668	0.0883	-4545 ± 72
0.6757	-14440 ± 626	0.0940	-49952 ± 682	0.0997	-5162 ± 80
0.6847	-15378 ± 666	0.1053	-50891 ± 733	0.1109	-5780 ± 88
0.7012	-15195 ± 658	0.1164	-50707 ± 704	0.1219	-6384 ± 69
0.7162	-15503 ± 672	0.1273	-51015 ± 708	0.1326	-6977 ± 104
0.7427	-15479 ± 671	0.1380	-50991 ± 681	0.1433	-7568 ± 111
0.7497	-14992 ± 650	0.1485	-50504 ± 647	0.1537	-8134 ± 118
$T = 873$ K; first measurement; starting amount: $n_{\text{Ag}} = 1.9944 \times 10^{-3}$ mol; $n_{\text{Cu}} = 0.6236 \times 10^{-3}$ mol; $n_{\text{Sn}} = 45.5455 \times 10^{-3}$ mol					
					152
0.5701	-21187 ± 669	0.0058	-51159 ± 991	0.0116	-447 ± 12
0.5162	-21731 ± 687	0.0167	-51703 ± 1128	0.0218	-1014 ± 24
0.5665	-21908 ± 692	0.0272	-51880 ± 1038	0.0327	-1612 ± 36
0.8113	-22802 ± 720	0.0401	-52774 ± 759	0.0476	-2441 ± 48
0.8229	-22080 ± 698	0.0549	-52052 ± 721	0.0621	-3248 ± 59
1.0979	-22729 ± 718	0.0714	-52701 ± 559	0.0807	-4279 ± 69
0.6052	-23010 ± 727	0.0856	-52981 ± 1029	0.0905	-4860 ± 80
0.2324	-22454 ± 709	0.0922	-52426 ± 2604	0.0939	-5075 ± 91
$T = 873$ K; second measurement; starting amount: $n_{\text{Ag}} = 1.8391 \times 10^{-3}$ mol; $n_{\text{Cu}} = 0.5751 \times 10^{-3}$ mol; $n_{\text{Sn}} = 41.9986 \times 10^{-3}$ mol					
					152
0.2662	-21613 ± 474	0.0030	-51585 ± 1005	0.0059	-157 ± 9
0.2395	-21910 ± 481	0.0086	-51882 ± 1135	0.0112	-450 ± 19
0.4425	-22942 ± 484	0.0159	-52014 ± 619	0.0207	-962 ± 28
0.3227	-22008 ± 483	0.0240	-51980 ± 847	0.0273	-1341 ± 37
0.5358	-22191 ± 487	0.0327	-52163 ± 515	0.0382	-1931 ± 46
0.7365	-22375 ± 491	0.0454	-52347 ± 378	0.0526	-2723 ± 54
0.5059	-21987 ± 483	0.0573	-51959 ± 539	0.0620	-3261 ± 62
0.6155	-22840 ± 501	0.0675	-52811 ± 464	0.0731	-3881 ± 69
0.2582	-22827 ± 501	0.0753	-52799 ± 1105	0.0775	-4152 ± 78

^a Average of x_{Ni} before and after drop. ^b Per mole of the mixture.

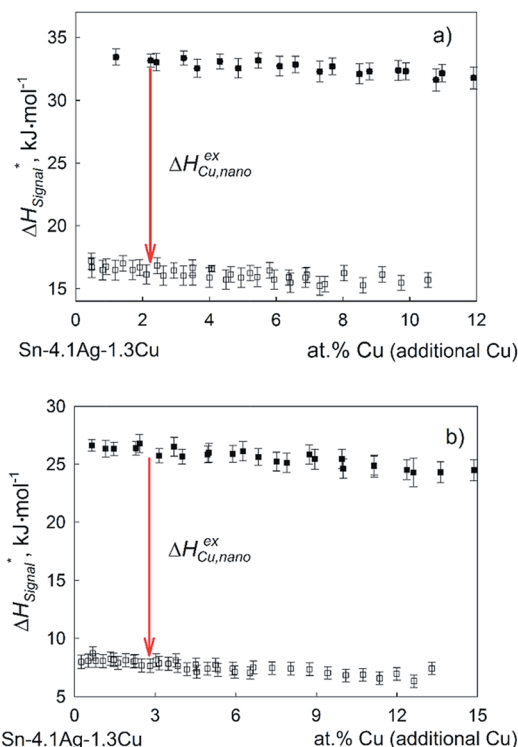


Fig. 5 Concentration dependencies of the measured enthalpy effect for (Sn-4.1Ag-1.3Cu)_{100-x}Cu_x at 1073 K (a) and 873 K (b) (■ – for additions of bulk Cu; □ – for additions of nanosized Cu).

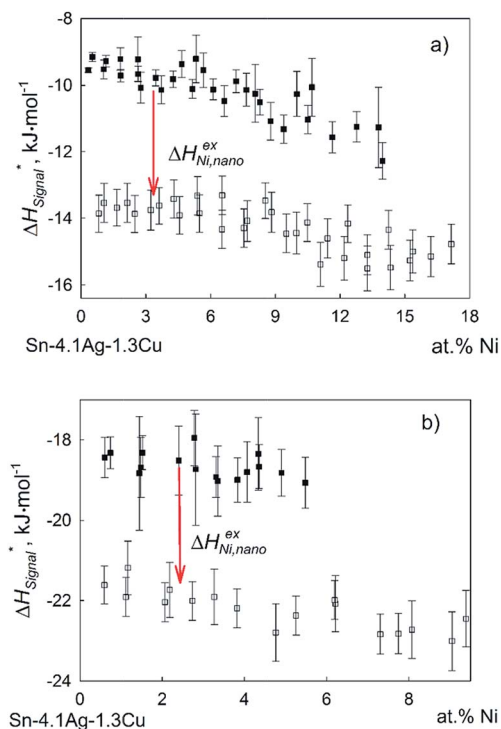


Fig. 6 Concentration dependencies of the measured enthalpy effect for (Sn-4.1Ag-1.3Cu)_{100-x}Ni_x at 1073 K (a) and 873 K (b) (■ – for additions of bulk Ni; □ – for additions of nanosized Ni).

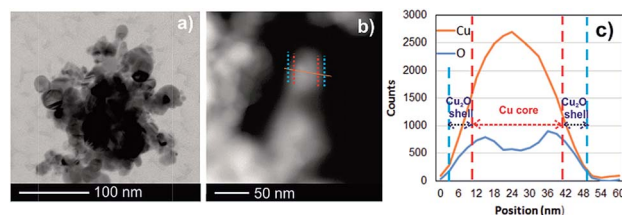


Fig. 7 TEM bright field image (a) and HAADF STEM image (b) with corresponding EDX linescan (c) of Cu NPs.

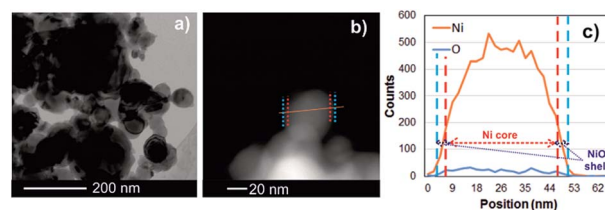


Fig. 8 TEM bright field image (a) and HAADF STEM image (b) with corresponding EDX linescan (c) of Ni NPs.

the total molar amount of substance, where n_j stands for the molar amount of substance which was already present in the crucible:

$$\Delta_{\text{Mix}}H = \frac{\sum \Delta H_{\text{Reaction}}}{n_j + \sum n_i} \quad (13)$$

Prior to the measurements, the SAC387 alloy was prepared from Sn ingot (99.998% metallic purity), Ag shot (99.999% metallic purity) and Cu rods (99.9% metallic purity, all from Alfa Aesar, Karlsruhe, Germany) without further purification. The samples with a total mass between 5 and 10 g were sealed in evacuated quartz glass ampoules and kept in a muffle furnace for 2 weeks at 1173 K. The mass loss of the ingots was less than 0.1 mg.

The measurements were performed by dropping pure Ni or Cu, both in bulk and nanosized form. Ni pieces were obtained from Advent (99.99%; Oxford, UK), Ni and Cu nanopowders from IoLiTec Nanomaterials (Heilbronn, Germany). To avoid severe oxidation, all operations with nano-Ni and nano-Cu were

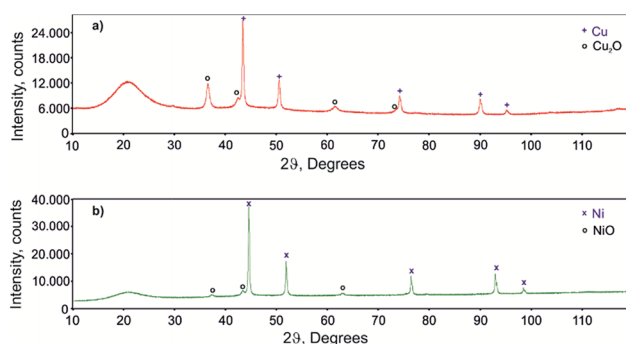


Fig. 9 XRD patterns of Cu (a) and Ni NPs (b).



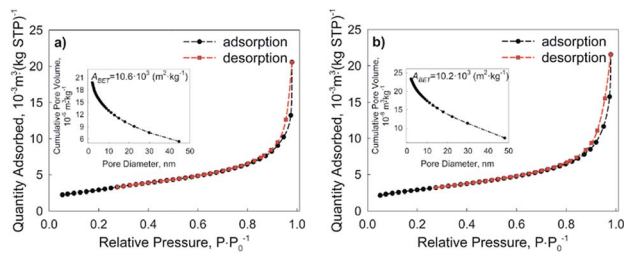


Fig. 10 BET isotherm and BJH pore size distribution of Cu (a) and Ni NPs (b).

performed in a glovebox (M. Braun, LabMaster 130) under Ar atmosphere (Ar 5.0; O₂ and H₂O < 5 ppm each). The calorimetric measurements using the metal nanopowders were carried out similar to our previous thermodynamic investigations of nano-Co additions to liquid SAC387 alloys.¹⁹ The Ni and Cu nanoparticles were first packed into a SAC387 foil. The employed foil was produced from the same ingot using a foil rolling mill; it had a thickness of about 50 μm. The sample holders of the auto sampling device were loaded with nanopowder samples inside the glovebox and closed in a box, which was only taken out just before the measurement to be transported to the calorimeter. The calorimetric measurements with the packed nanoparticles were started with five drops of SAC387 foil pieces in order to determine and, subsequently, subtract the heat effect of the SAC387 foil from the obtained measured enthalpy. A few measurements with bulk Cu and Ni, packed into the SAC387 foil, were also carried out to prove the accuracy of this procedure.

Various factors must be considered when estimating the random and systematic errors in the measurements, *i.e.* the calorimeter construction, measuring method, calibration procedure, signal integration and “chemical errors”. Uncertainties of the enthalpy values given in Tables 1–6 were estimated based on the propagation of errors, taking also into account the standard deviation of the calorimeter constant $s(k)$

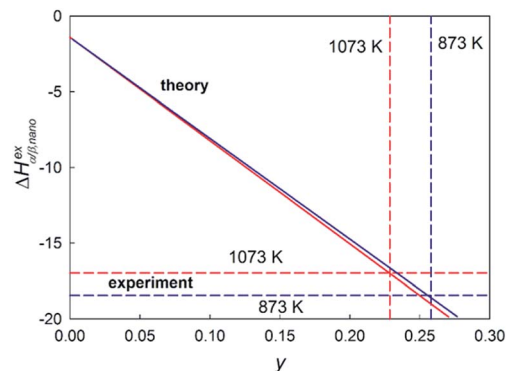


Fig. 11 Comparison of experimental data (dotted horizontal lines) with theoretical values (bold lines) at two temperatures for the dependence of the excess nano enthalpy effect on the ratio of oxidation of the Cu nanoparticles. Calculated by eqn (5)–(7) and (9) and parameters of Table 8.

which was evaluated by five drops of alumina for each run. The uncertainty of the partial enthalpy of mixing for each drop was calculated based on the uncertainties of peak areas of each drop, A_i , of the amount of added component, n_i , and $s(k)$; the error of the integrated enthalpy of mixing was taken summarizing the errors of the single drops throughout the final composition. A similar procedure of calculation of the uncertainties of the enthalpy values was employed previously in ref. 44 and 45.

The phase composition and the microstructure of the samples were examined after the calorimetric measurements by powder X-ray diffraction (XRD; Bruker D8 Advance X-ray diffractometer) and scanning electron microscopy (SEM; Zeiss Supra 55 ESEM). The XRD analysis was carried out at ambient temperature using Ni-filtered Cu K α radiation (accelerating voltage 40 kV, electron current 40 mA). The nanopowders were fixed onto the sample holder using pre-dried petroleum jelly in the Ar-filled glovebox. Rietveld refinement of XRD patterns was performed with the Topas 3 software provided by Bruker AXS.

Table 7 Calculated and measured nano-effects ($\Delta H_{i,nano}^{ex}$, kJ mol⁻¹) without considering the influence of the oxide shell on the nano-particles

Metal	A_{BET} (m ² g ⁻¹)	M (g mol ⁻¹)	σ_{sg,H,T_D} (J m ⁻²) ³⁵	$\Delta H_{i,nano}^{ex}$ eqn (1)	$\Delta H_{i,nano}^{ex}$ experiment
Cu	10.6 ± 0.4	63.55	1.93 ± 0.19	-1.3 ± 0.2	-17.8 ± 0.8
Ni	10.2 ± 0.4	58.69	2.36 ± 0.23	-1.4 ± 0.2	-3.5 ± 0.3

Table 8 Parameters to calculate the excess nano heat effect $\Delta H_{i,nano}^{exp}$ (kJ mol⁻¹) by eqn (4)–(7) and (9)^a

Metal	A_{BET} (m ² g ⁻¹)	M_α (g mol ⁻¹)	β_x	M (g mol ⁻¹)	ρ_β (g cm ⁻³)	σ_{α,H,T_D} (J m ⁻²)	σ_{β,H,T_D} (J m ⁻²)	$\sigma_{\alpha/\beta,H,T_D}$ (J m ⁻²)	T (K)	ΔH_{C_p} (kJ mol ⁻¹)	$\Delta_r H^0$ (kJ mol ⁻¹)
Cu	10.6	63.55	0.5	71.55	6.0	1.93	0.7	1.93	873	6.00	-71.05
Cu	10.6	63.55	0.5	71.55	6.0	1.93	0.7	1.93	1073	8.40	-75.01
Ni	10.2	58.69	1	74.69	7.45	2.36	0.9	2.36	873	13.96	-61.84
Ni	10.2	58.69	1	74.69	7.45	2.36	0.9	2.36	1073	18.208	-64.33

^a Density is from ref. 39, interfacial energies are from ref. 35 and 40, and enthalpy data are from ref. 41.



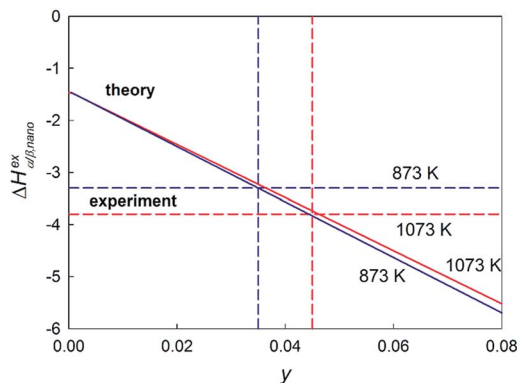


Fig. 12 Comparison of experimental data (dotted horizontal lines) with theoretical values (bold lines) for the dependence of the excess nano enthalpy effect on the ratio of oxidation of the Ni nanoparticles. Calculated by eqn (4)–(7) and (9) and parameters of Table 8.

The energy-dispersive X-ray (EDX) detector signal for SEM analysis was calibrated using pure elements as standard materials and Co for the energy calibration.

The Ni and Cu nanoparticles were characterized by XRD analysis (XRD; Bruker D8 Advance X-ray diffractometer) and transmission electron microscopy (TEM; analytical TECNAI F20 field emission TEM). A silicon single crystal sample holder with a matching polymer (polycarbonate) cap was used in order to avoid a possible oxidation of NPs. The EDX mapping of NPs was performed with an energy-dispersive X-ray detector (EDAX TEAM Apollo XLTW SDD).

The surface area of the nanopowders was estimated using the BET technique, whereby N_2 adsorption-desorption isotherms of the nanopowders were analyzed using a TriStar II 3020 instrument (Micromeritics). This method is based on a theory developed by S. Brunauer, P. Emmett and E. Teller⁴⁶ where the name of the theory was taken from the first letter of each author's surnames. According to this method, the surface area of a known mass of a sample was determined by monitoring the mass change by adsorption of nitrogen over time, which is widely used due to its availability in high purity and its strong interaction with most solids. The data collected during the measurement are shown in the form of a BET isotherm, which plots the quantity of gas adsorbed as a function of the relative pressure.

Conclusions

The presented experimental results show clearly that an extra exothermic heat effect (nano-heat effect) is observed when bulk pieces are replaced by nano-particles in drop calorimetric measurements. First of all, this is due to the loss of the large surface area of the nano-particles upon their dissolution. However, when the nano-particles are covered with a surface oxide shell, resulting in an exothermic chemical reaction with the solvent (a liquid alloy in the present case), the measured nano-effect can become even more exothermic, especially if the reaction enthalpy is strongly negative. This effect has been

examined here on the example of the core/shell Cu/Cu₂O and Ni/NiO nano-particles dropped into Sn-rich liquid alloys.

Conflicts of interest

There are no conflicts to declare.

Acknowledgements

This work was supported by the Austrian Science Fund (FWF) [grant numbers P 26304 and P 27049]. The authors want to acknowledge the help of Prof. M. Zehetbauer and Prof. E. Schafner from the Faculty of Physics, University of Vienna, with the Sn-4.1Ag-1.3Cu foil preparation, Ing. C. Mitterer from the Faculty of Chemistry, University of Vienna, with BET analysis and Dr St. Puchegger from the Faculty of Physics, University of Vienna, with the SEM studies. TEM analysis was performed using the facilities at the University Service Center for Transmission Electron Microscopy at the Vienna University of Technology. The work by G.K. was supported by project GINOP 2.3.2 – 15 – 2016 – 00027 financed in the framework of the Széchenyi-plan supported by the European Union.

References

- 1 M. Zhang, M. Y. Efremov, F. Schiettekatte, E. A. Olson, A. T. Kwan, S. L. Lai, T. Wisleder, J. E. Greene and L. H. Allen, *Phys. Rev. B*, 2000, **62**, 10548–10557.
- 2 S. Y. Xiong, W. H. Qi, Y. J. Cheng, B. Y. Huang, M. P. Wang and Y. J. Li, *Phys. Chem. Chem. Phys.*, 2011, **13**, 10652–10660.
- 3 R. Ferrando, *Structure and properties of nanoalloys*, Elsevier, Amsterdam, 2016, vol 10.
- 4 Y. Hua, K. Chandra, D. H. M. Dam, G. P. Wiederrecht and T. W. Odom, *J. Phys. Chem. Lett.*, 2015, **6**, 4904–4908.
- 5 K. S. Lee and M. A. El-Sayed, *J. Phys. Chem. B*, 2006, **110**, 19220–19225.
- 6 N. Dai, L. Zhang, Z. Wang, X. Wang, J. Zhang, H. Gong, H.-B. Han and Y. Han, *J. Phys. Chem. C*, 2017, **121**, 12358–12364.
- 7 I. Papagiannouli, P. Aloukos, D. Rioux, M. Meunier and S. Couris, *J. Phys. Chem. C*, 2015, **119**, 6861–6872.
- 8 S. W. Baek, G. Park, J. Noh, C. Cho, C. H. Lee, M. K. Seo, H. Song and J. Y. Lee, *ACS Nano*, 2014, **8**, 3302–3312.
- 9 E. Hao, G. C. Schatz and J. T. Hupp, *J. Fluoresc.*, 2004, **14**, 331–341.
- 10 W. H. Qi, *Acc. Chem. Res.*, 2016, **49**, 1587–1595.
- 11 J. Shen and Y. C. Chan, *Microelectron. Reliab.*, 2009, **49**, 223–234.
- 12 L. Sun and L. Zhang, *Adv. Mater. Sci. Eng.*, 2015, **2015**, 639028.
- 13 E. E. M. Noor, A. Singh and T. C. Yap, *Soldering Surf. Mount Technol.*, 2013, **25**, 229–241.
- 14 A. Yakymovych, Y. Plevachuk, P. Svec, D. Janikovic, P. Sebo, N. Beronska, M. Nosko, L. Orovcik, A. Roshanghias and H. Ipser, *J. Mater. Sci.: Mater. Electron.*, 2017, **28**, 10965–10973.



- 15 M. N. Bashir, A. S. M. A. Haseeb, A. M. S. Rahman, M. A. Fazal and C. R. Kao, *J. Mater. Sci.*, 2015, **50**, 6748–6756.
- 16 A. K. Gain and Y. C. Chan, *Intermetallics*, 2012, **29**, 48–55.
- 17 L. Zhang and K. N. Tu, *Mater. Sci. Eng., R*, 2014, **82**, 1–32.
- 18 S. L. Tay, A. S. M. A. Haseeb, M. R. Johan, P. R. Munroe and M. Z. Quadir, *Intermetallics*, 2013, **33**, 8–15.
- 19 A. Yakymovych, G. Kaptay, A. Roshanghias, H. Flandorfer and H. Ipser, *J. Phys. Chem. C*, 2016, **120**, 1881–1890.
- 20 A. Yakymovych, Y. Plevachuk, V. Sklyarchuk, B. Sokoliuk, T. Galya and H. Ipser, *J. Phase Equilib. Diffus.*, 2017, **38**, 217–222.
- 21 A. Yakymovych, S. Mudry, I. Shtablayvi and H. Ipser, *Mater. Chem. Phys.*, 2016, **181**, 470–475.
- 22 A. T. Tan, A. W. Tan and F. Yusof, *Sci. Technol. Adv. Mater.*, 2015, 16.
- 23 H. Flandorfer, C. Luef and U. Saeed, *J. Non-Cryst. Solids*, 2008, **354**, 2953–2972.
- 24 C. Luef, H. Flandorfer and H. Ipser, *Z. Metallkd.*, 2004, **95**, 151–163.
- 25 G. Kaptay, *Metall. Mater. Trans. A*, 2012, **43**, 531–543.
- 26 U. Saeed, H. Flandorfer and H. Ipser, *J. Mater. Res.*, 2007, **22**, 3218–3225.
- 27 S. W. Chen and C. A. Chang, *J. Electron. Mater.*, 2004, **33**, 1071–1079.
- 28 C. Schmetterer, M. Rodriguez-Hortala and H. Flandorfer, *J. Phase Equilib. Diffus.*, 2014, **35**, 429–433.
- 29 S. Furtauer, D. Li, D. Cupid and H. Flandorfer, *Intermetallics*, 2013, **34**, 142–147.
- 30 W. Wang, Z. G. Liao, Y. Wang, X. A. Wu, F. Y. Qu and X. Zhang, *Cryst. Res. Technol.*, 2011, **46**, 300–304.
- 31 P. E. Tomaszewski, *Phase Transitions*, 1992, **38**, 127–220.
- 32 R. Vallee, M. Wautelet, J. P. Dauchot and M. Hecq, *Nanotechnology*, 2001, **12**, 68–74.
- 33 G. Kaptay, *J. Nanosci. Nanotechnol.*, 2012, **12**, 2625–2633.
- 34 G. Kaptay, *RSC Adv.*, 2017, **7**, 41241–41253.
- 35 L. Z. Mezey and J. Giber, *Jpn. J. Appl. Phys., Part 1*, 1982, **21**, 1569–1571.
- 36 G. Kaptay, *J. Mater. Sci.*, 2012, **47**, 8320–8335.
- 37 R. D. Holmes, H. S. C. O'Neill and R. J. Arculus, *Geochim. Cosmochim. Acta*, 1986, **50**, 2439–2452.
- 38 G. Petot-Ervas, R. Farhi and C. Petot, *J. Chem. Thermodyn.*, 1975, **7**, 1131–1136.
- 39 G. V. Samsonov, *Physico-chemical properties of oxides, Metallurgia*, Moscow, 1978.
- 40 G. Kaptay, E. Bader and L. Bolyan, *Mater. Sci. Forum*, 2000, **329–3**, 151–156.
- 41 I. Barin and F. Sauert, *Thermochemical properties of pure substances*, Wiley-VCH, New York, 1993.
- 42 H. Flandorfer, F. Gehringer and E. Hayer, *Thermochim. Acta*, 2002, **382**, 77–87.
- 43 A. T. Dinsdale, *CALPHAD*, 1991, **15**, 317–425.
- 44 A. Yakymovych, S. Furtauer, H. Flandorfer and H. Ipser, *Monatsh. Chem.*, 2014, **145**, 1697–1706.
- 45 A. Yakymovych, S. Furtauer, A. Elmahfoudi, H. Ipser and H. Flandorfer, *J. Chem. Thermodyn.*, 2014, **74**, 269–285.
- 46 S. Brunauer, P. H. Emmett and E. Teller, *J. Am. Chem. Soc.*, 1938, **60**, 309–319.

